**RESEARCH**

# Intelligent interference cancellation and ambient backscatter signal extraction for wireless-powered UAV IoT network

Cheng Zhong[1], Di Zhai[2], Yang Lu[2] and Ke Li[3]*

*Correspondence:
keli_like2023@163.com

[1] State Grid Xiongan New Area
Electric Power Supply Company,
Heibei 0710002, China
[2] State Grid Smart Grid Research
Institute Co.Ltd., Beijing 102209,
China
[3] University of Science
and Technology Beijing, 30
Xueyuan Road, Haidian District,
Beijing 100083, China

## Abstract

Unmanned aerial vehicles (UAVs) offer a new approach to wireless communication, leveraging their high mobility, flexibility, and visual communication capabilities. Ambient backscatter communication enables Internet of Things devices to transmit data by reflecting and modulating ambient radio waves, eliminating the need for additional wireless channels, and reducing energy consumption and cost for sensors. However, passive ambient backscatter communication has limitations such as limited range and poor communication quality. By utilizing UAVs as communication nodes, these limitations can be overcome, expanding the communication range and improving the quality of communication. Although some research has been conducted on combining UAVs and ambient backscatter, several challenges remain. One key challenge is the strong direct link interference in ambient backscatter under UAV conditions, which significantly affects communication quality. In this paper, we propose an intelligent backward and forward straight link interference cancellation algorithm based on NOMA decoding technique to enhance ambient backscatter communication quality under UAV conditions and extract more ambient energy for UAV energy supply. The paper includes theoretical derivation, algorithm description, and simulation analysis to validate the error bit rate of labeled information bits. The results demonstrate that the forward algorithm reduces the error bit rate by approximately 20% under low signal-to-noise ratio (SNR) conditions, while the backward algorithm reduces the error bit rate under high SNR conditions. The combination of the forward and backward algorithms reduces the error bit rate under both high and low SNR conditions. The proposed method contributes to improving the quality of ambient backscatter communication in UAV settings.

**Keywords:**  Unmanned aerial vehicle, Ambient backscatter, Iterative algorithm, Energy harvesting

## 1 Introduction

In recent years, there has been a growing interest among researchers in unmanned aerial vehicles (UAVs) due to their exceptional characteristics, such as rapid deployment, terrain independence, high flexibility, and mobility. By utilizing UAVs as communication nodes, it is possible to extend the communication range and establish visual channels

to improve communication quality. A multi-UAV enabled mobile Internet of Vehicles (IoV) model is proposed in [1] which achieve the excellent performance of the multi-UAV enabled mobile IoV. A method was proposed to improve communications security via optimizing power allocation, RIS passive beamforming, and UAV trajectory [2]. Additionally, UAV communication holds great potential in challenging environments such as mountainous regions, disaster areas, and deserts. This form of communication presents both opportunities and challenges in wireless communication and the Internet of Things (IoT). The Internet of Everything (IoE) typically employs 5G technologies, enabling the seamless transmission of information and interaction among multiple low-power devices within a specific area [3, 4].

Ambient backscatter communication (AmBC), among various 5G technologies, enables low-power Internet of Everything by allowing multiple tags of an access device to transmit data through reflection or modulation of ambient radio waves without occupying additional wireless channels. This technology significantly reduces sensor energy consumption and costs. Ambient backscattering also encompasses the feature of energy harvesting, wherein passive tags gather surrounding ambient RF signals (e.g., WiFi and TV broadcast signals) to obtain energy without requiring oscillating circuits for signal generation. The communication system in ambient backscatter typically comprises a transceiver (RF source and reader) and a tag (backscatter node). Unlike conventional wireless communication systems, the tag does not actively transmit signals, instead, it receives a backscatter coefficient carrier signal modulated from the RF source and reflects it. In this way, the signal from a passive tag in an ambient backscatter system is an RF signal modulated by altering the tag's antenna impedance. When the tag is in a backscattered state, it sends a "1," and when it is in a non-backscattered state, it sends a "0" [5, 6].

However, due to the passive nature of ambient backscatter, the reflected signal from the tag introduces an additional fading effect on the channel during transmission, resulting in a weaker received signal strength. Consequently, the communication range and network size of ambient backscatter systems are comparatively smaller than those of conventional active communication systems. The characteristics of UAV-assisted communication can effectively compensate for these limitations of ambient backscatter communication. Furthermore, traditional IoT devices often require periodic charging or battery replacement, creating inconvenience for wireless devices, especially those deployed in harsh environments. With the rapid expansion of the IoT and the proliferation of access devices across diverse environments, maintaining battery-dependent devices becomes resource-intensive and challenging. Ambient backscatter communication techniques present effective solutions for overcoming these limitations, and research has been conducted on harnessing ambient radio frequency (RF) signals for energy supply [7]. In an ambient backscatter system, RF signals from the environment serve as an energy source to sustain the operation of low-power devices. This system not only facilitates wireless information transmission but also enables simultaneous transmission of wireless information and electrical energy [8]. Additionally, since tags in ambient backscatter do not require oscillating circuits to generate carrier signals, the circuits can be simplified, and the energy required for circuit maintenance is significantly reduced, making zero-power communication feasible for the tags.

UAVs are energy-constrained devices, and therefore, they require efficient communication technologies to maximize communication efficiency during their operational hours. A fair energy-efficient resource optimization scheme for the IoT in [9] is studied to ensure fair energy consumption of multiple UAVs. NOMA (non-orthogonal multiple access), a key technology for 5G [10], plays a crucial role in achieving the Internet of Everything. In contrast with orthogonal frequency-division multiplexing (OFDM), where each orthogonal subcarrier conveys the information of a single user, NOMA optimally utilizes spectrum resources by transmitting multiple users' information in a single subcarrier through power differences. This necessitates more sophisticated resource allocation strategies, and multi-access interference is an inherent challenge in NOMA technology. To address excessive interference, users assigned to the same resource need to be multiplexed appropriately, and techniques like successive interference cancellation (SIC) are required to ensure reliable communication [11]. Integrating AmBC and NOMA schemes under UAV conditions offers a promising solution to meet communication requirements in specific IoT scenarios. Existing literature primarily focuses on backscatter-assisted NOMA systems for various system scenarios [12–14]. For example, [15] presents a criterion for selecting a reflection coefficient in SIC-based NOMA backscatter systems and emphasizes the significance of applying NOMA to AmBC systems. The proposed solution in [16] combines random channel access and SIC, offering an efficient NOMA scheme for single-site backscatter systems. Moreover, [17, 18] propose the use of backscatter for collaborative NOMA downlinks, demonstrating significant improvements in energy efficiency and transmission reliability [17, 18].

Due to payload limitations, UAVs cannot carry bulky and complex signal processing equipment. As a result, mitigating the adverse effects of direct link interference (DLI) in UAV-conditioned ambient backscatter communications poses a challenge, and existing interference elimination techniques are mostly unsuitable for UAV-conditioned ambient backscatter systems. Current studies primarily examine ground-based ambient backscatter communication systems and treat DLI as background noise when decoding the backscatter signal (BS). For instance, maximum-likelihood (ML) detection for AmBC communication systems is investigated in [19]. However, strong DLI results in low signal-to-interference-plus-noise ratio (SINR) of the received output signal, limiting the transmission rate. Various techniques, such as frequency shifting, have been suggested in [20–22] to allocate non-overlapping sub-channels to the BS for interference-free transmission. Nevertheless, dedicating frequency bands for BS transmission consumes additional spectral resources, thereby reducing spectral efficiency. Joint detection approaches, where the BS is jointly decoded with DLI, have been proposed in [23–25], necessitating joint design and precise time synchronization between the BS and DLI. Additionally, [26] investigates multi-antenna cancellation of DLI by introducing diversity gain; however, it is not applicable to single-antenna ambient backscatter communication systems. Furthermore, ML detector-based DLI cancellation techniques for OFDM-based ambient RF sources require special waveform designs [27, 28], and self-interference cancellation techniques which incorporate an ambient backscatter receiver into the ambient RF source require special transceiver designs [29–31]. Similarly, continuous interference cancellation-based detection has been proposed in [32] to separate the BS from DLI by decoding the DLI first and then subtracting it from the mixed reception at the AmBC receiver. However, all these methods treat

DLI as interference and have certain limitations. Moreover, the complexity of receiver and waveform designs limits their applicability to UAV conditions.

In this paper, based on AmBC under UAV conditions, and considering inherent challenges such as NOMA's inability to completely eliminate strong direct link interference, we propose an intelligent backward and forward algorithm that exploits the inherent backward and iterative characteristics of the signal. The proposed algorithm treats DLI as a signal throughout the entire process. It first performs initial signal separation through NOMA decoding and then utilizes historical signals for iterative separation of the received signal. The labeling information is verified using the forward and backward algorithms, reducing the false bit rate. Furthermore, the separated interference signal can be fed into an energy extractor for energy harvesting, thus achieving the integration of passive communication, interference elimination, and ambient energy extraction.

## 2 System model and interference analysis

### 2.1 System model

An ambient backscatter system under UAV conditions (AUAV) comprises an RF source, a stationary reflective tag, and a reader (UAV) as the receiver. The RF source broadcasts RF signals that can be received both by the tag and the reader. The direct signal from the RF source to the reader is reflected by the tag, resulting in strong direct link interference. The RF source signal also reaches the tag, which modulates its own information onto the incident RF signal for transmission. Consequently, the received signal at the reader is a combination of the direct signal and the reflected signal (Fig. 1).

The direct signal component arriving at the UAV from the RF source is given by

$$x_{\mathrm{sr}}(t) = \sqrt{P_t}h_2 s(t - \tau_2). \tag{1}$$

The signal component arriving at the tag from the RF source is expressed as

$$x_{\mathrm{st}}(t) = \sqrt{P_t}h_1 s(t - \tau_1) + n_{st}(t). \tag{2}$$

Due to the tag's primary backscatter operation and minimal signal processing, the noise at the tag can be neglected. Therefore, the signal component reflected by the tag and reaching the UAV is



| $h$ | channel fading coefficient |
| $\tau$ | time delay |
| $d$ | distance |
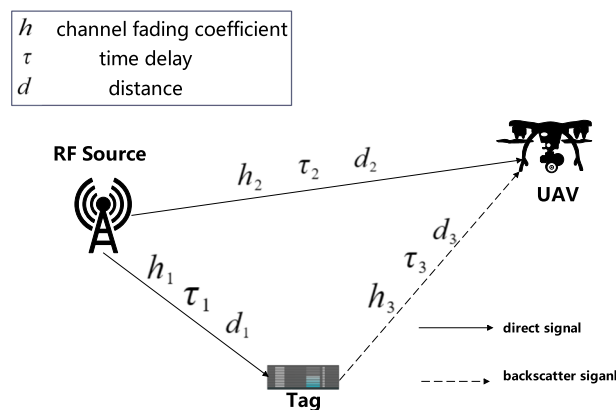
**Fig. 1** Ambient backscatter system under UAV's condition

$$x_{\text{tr}}(t) = \sqrt{\alpha\eta}h_3c(t - \tau_3)x_{\text{st}}(t - \tau_3), \tag{3}$$

where $P_t$ denotes the transmit power of the RF signal, and $s(t)$ represents the normalized signal with $\|s(t)\|^2 = 1$, $\alpha$ represents the tag antenna's reflection coefficient, $\eta$ signifies the reflection efficiency of the tag circuit, and $c(t) \in \{-1, 1\}$ denotes the backscatter data or tag bit transmitted by the tag. Likewise, $h_1$, $d_1$, $h_2$, $d_2$, $h_3$, and $d_3$ refer to the channel fading coefficients and the distances between the RF source and the tag, the RF source and the UAV, and the tag and the UAV, respectively. Furthermore, $\tau_1$, $\tau_2$, and $\tau_3$ represent the delay of the transmitted signal through the channels $h_1$, $h_2$, and $h_3$ respectively. Each distance is proportional to its respective time delay. $n_{st}(t)$ and $n(t)$ denote additive Gaussian white noise with a dual-power spectral density of $\sigma^2$. As a result, the received signal at the UAV is given by

$$y_r(t) = x_{tr}(t) + x_{sr}(t) + n(t). \tag{4}$$

## 2.2 Signal-to-interference-plus-noise ratio and inter-symbol interference analysis

The received signal at the UAV can be expressed as

$$y_r(t) = s_1(t) + s_2(t) + N(t), \tag{5}$$

where $s_1(t) = \sqrt{P_t}h_2s(t - \tau_2)$, $s_2(t) = \sqrt{\alpha\eta}h_3c(t - \tau_3)\sqrt{P_t}h_1s(t - \tau_1 - \tau_3)$, $N(t) = n(t) + \sqrt{\alpha\eta}h_3c(t - \tau_3)n_{st}(t)$ represents the noise. When decoding $c(t)$ from $y_r(t)$, the received signal-to-interference-and-noise ratio (SINR) is given by

$$\gamma = \frac{P_t\alpha\eta|h_3|^2|h_1|^2}{P_t|h_2|^2 + (1 + \alpha\eta|h_3|^2)\sigma^2}. \tag{6}$$

Analysis of the above equation reveals that increasing the transmit power leads to an increase in the power of the reflected signal, which represents the useful signal. However, it also amplifies the power of the strong direct link interference, thereby reducing the signal-to-noise ratio at the receiver. This, in turn, increases the bit error rate (BER) under low signal-to-noise ratio conditions, resulting in a decline in communication quality. Hence, simply increasing the transmit power is insufficient to solve the problem. As the reflected signal and the direct signal take different paths and experience different delays, the problem can be effectively transformed into an inter-symbol interference (ISI) problem by separately analyzing the signal and the direct link interference at the receiver.

Assuming that channel conditions remain constant over a short period, the channel fading coefficient can be considered as a constant. $\alpha$ and $\eta$ are constants, and the binary symbol $c(t)$, which can be treated as a special amplitude gain, is also constant. Thus, Eq. (3) can be reduced to

$$x_{tr}(t) = \sqrt{P_t}\tilde{h}_3s(t - \tau), \tag{7}$$

where $\tilde{h}_3 = \sqrt{\alpha\eta}h_3c(t - \tau_3)h_1$ and $\tau = \tau_1 + \tau_3$.

Compared to Eq. (1), the reflected signal can be considered as inter-symbol interference caused by the direct link interference. Therefore, the received signal at the UAV can be written as

$$y_r(t) = s_1(t) + \underbrace{x_{tr}(t)}_{\text{ISI}} + N(t). \tag{8}$$

The reflected signals serve as both useful signals and inter-code interference. By eliminating the strong direct link interference from the received signal at the reader, the problem of decoding the tag information in the reflected signals can be solved.

## 3 Methods to eliminate strong DLI

### 3.1 Discussion of special cases

First, let's consider some special cases involving $s(t)$ as the focus of our study. If $\tau_2 = \tau_1 + \tau_3$, which means $d_2 = d_1 + d_3$, then Eq. (8) can be simplified as

$$y_r(t) = \sqrt{P_t}(h_2 + \tilde{h}_3)s(t - \tau) + N(t). \tag{9}$$

In such a case, there is no interference. If $c(t - \tau_3) = 0$, then the received signal can be written as

$$y_r(t) = \sqrt{P_t}h_2 s(t - \tau_2) + N(t). \tag{10}$$

In this case, there is only DLI, and decoding the reflected signal and the backscatter data becomes straightforward.

Next, we consider $c(t - \tau_3)$ as the focus of our study. If $s(t - \tau_2) = 0$, then Eq. (8) reduces to

$$y_r(t) = \sqrt{P_t}\tilde{h}_3 s(t - \tau) + N(t), \tag{11}$$

which means that there is no DLI, and the label bit can be decoded directly. If $s(t - \tau) = 0$, the equation can be expressed as

$$y_r(t) = \sqrt{P_t}h_2 s(t - \tau_2) + N(t), \tag{12}$$

this is the same as the case in Eq. (11). In the case of the special scenario described above, we can easily get the label information, we need from the received signal without complex decoding.

### 3.2 Forward and backward decoding

The final received signal at the UAV is given by Eq. (8). Considering the substantial power difference between the direct link signal and the tag reflection signal due to the tag reflection efficiency and the reflection coefficient, we can use the successive interference cancellation (SIC) technique to decode $s_1(t)$ first and then obtain $x_{tr}(t)$ to decode the tag bit $c(t - \tau_3)$. The received signal $y_r(t)$, the RF source signal $s(t)$, and the tag bit $c(t)$ are stored in memory at each time point. However, SIC decoding, based on power, may introduce errors in the backscatter data. Therefore, a backward decoding process is performed to verify the tag bit.

First, we construct an inter-symbol interference (ISI) in Eq. (8) using the known signals

$$x_{tr}(t) = \frac{\tilde{h}_3}{h_2}[y_r(t + \tau_2 - \tau) - s_f^*(t) - N(t + \tau_2 - \tau)], \tag{13}$$

where $s_f^*(t) = \sqrt{\alpha\eta P_t}h_3h_1c(t - \tau_3 + \tau_2 - \tau)s(t + \tau_2 - 2\tau)$, assuming that the symbol period during tag modulation is longer than the RF source signal period, we can assume that the time interval between $c(t - \tau_3)$ and $c(t - \tau_3 + \tau_2 - \tau)$ is very small, and they represent the same symbol. By substituting Eq. (13) into Eq. (8), we have

$$y_r(t) - y_{tr}^*(t) = s_1(t) - s_{tr}^*(t) + N^*(t), \tag{14}$$

where $y_{tr}^*(t) = [\sqrt{\alpha\eta}h_3c(t - \tau_3)h_1y_r(t - \tau_0)]/h_2$,     $s_{tr}^*(t) = [\sqrt{P_t}\alpha\eta h_3{h_1}^2 s(t - \tau_0 - \tau)]/h_2$, $N_k^*(t) = N^*(t - 2k\tau_0)$, $k \in \{1, 2, 3...\}$, $N^*(t) = [N(t) - \sqrt{\alpha\eta}h_3c(t - \tau_3)h_1N(t - \tau_0)]/h_2$, $\tau_0 = \tau - \tau_2$, and $t \geq \tau_0 + \tau$. After backward iteration, Eq. (14) can be reduced to

$$y_r(\tilde{t}) - y_r^*(\tilde{t}) = s_1(\tilde{t}) - s_{tr}^*(\tilde{t}) + N_k^*(t), \tag{15}$$

where $\tilde{t} = t - 2k\tau_0$ and $0 \leq [t - (2k + 1)\tau_0 - \tau] < 2\tau_0$. Therefore, using the stored signals and Eq. (1), we obtain $s(t - 2k\tau_0 - \tau_2)$ and then obtain $s[t - (2k - 1)\tau_0 - \tau_2]$, and so on, until we obtain $c(t - \tau_3)$.

**Algorithm 1** Backward algorithm

---

**Require:** Signal received at UAV $y_r(t)$. Label bit $c(t)$ and RF signal $s(t)$ decoded by using SIC. Calculate $s(t - 2k\tau_0 - \tau_2)$ through Eq.(15);
1: **for** int i=-2k to 0 **do**
2: Bring $s(t - i\tau_0 - \tau_2)$ into $y_r(t + i\tau_0)$ in Eq.(15), then calculate $s[t - (i - 1)\tau_0 - \tau_2]$;
3: **end for**
4: Use the known signal and the $s(t - \tau_0 - \tau)$ obtained by iteration to get label bit $c(t - \tau_3)$;

---

The DLI can be constructed using the known signals

$$s_1(t) = \frac{h_2}{h_3^*}[y_r(t - \tau_2 + \tau) - s_b^*(t) - N(t)], \tag{16}$$

where $h_3^* = \sqrt{\alpha\eta}h_3c(t - \tau_2 + \tau - \tau_3)h_1$ and $s_b^*(t) = \sqrt{P_t}h_2s(t - 2\tau_2 + \tau)$.

Thus, Eq. (8) can be expressed as

$$y_r(t) = y_b^*(t) + x_{tr}(t) + N'(t), \tag{17}$$

where $y_b^*(t) = [h_2y_r(t + \tau_0) - \sqrt{P_t}(h_2)^2s(t + \tau - 2\tau_2)]/h_3^*$, $N'(t) = [1 - h_2h_3^*]N(t)$.
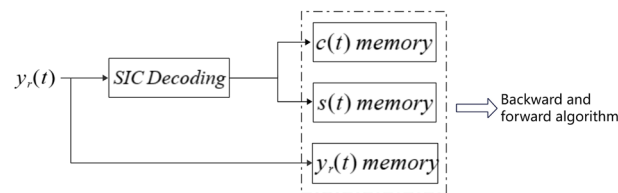
The signal received by the UAV at time $\tau$ contains both the direct link signal and the tag reflection signal:

$$y_r(\tau) = y_b^*(\tau) + x_{tr}(\tau) + N'(\tau). \tag{18}$$

After forward iteration, we have

$$y_r(t_k^{\tau_0}) = y_b^*(t_k^{\tau_0}) + x_{tr}(t_k^{\tau_0}) + N'(t_k^{\tau_0}), \tag{19}$$

**Fig. 2** System algorithm flow of AUAV

where $t_k^{\tau_0} = \tau + k\tau_0$. Eventually, we obtain $c(\tau - \tau_3 + k\tau_0)$. Once the decoding and verification of the tag signals are complete, the received signals and RF signals stored in memory can be used for energy extraction. The tag information memory can be used for other signal processing tasks (Fig. 2).

**Algorithm 2** Forward algorithm

---
**Require:** Signal received at UAV $y_r(t)$. Label bit $c(t)$ and RF signal $s(t)$ decoded by using SIC;
1: **for** int n=0 to k,$n \in \{1, 3, 5...\}$ **do**
2: Use the known signal and $y_r(\tau + n\tau_0)$ in Eq.(19) to get $s((n+2)\tau_0)$;
3: **end for**
4: Finally use the $s((k+2)\tau_0)$ obtained by iteration to get $c(\tau - \tau_3 + k\tau_0)$;
5: **for** int n=0 to k,$n \in \{0, 2, 4...\}$ **do**
6: Use the known signal and $y_r(\tau + n\tau_0)$ in Eq.(19) to get $s((n+2)\tau_0)$;
7: **end for**
8: Finally use the $s((k+2)\tau_0)$ obtained by iteration to get $c(\tau - \tau_3 + k\tau_0)$;

---

## 4 Numerical results

Figure 3 presents a comparison of the bit error rate (BER) of the ambient backscatter communication system decoded solely by SIC, the backward algorithm under, and the forward algorithm UAV conditions. It is apparent that the BER of the two algorithms is roughly the same at low signal-to-noise ratio (SNR), and the BER of the backward algorithm starts to decrease significantly when the BER exceeds 6. This effect can be attributed to the backward algorithm iteratively obtaining information from the previous moment to improve the accuracy of the current moment's labeling information. It is important to note that the SNR at this point is the ratio of the RF source signal to the noise, not the ratio of the tag reflection signal to the strong direct link interference signal, as the SIC decoding is performed first. This demonstrates that the backward algorithm has a positive impact on restoring tag information under high SNR conditions.

The forward algorithm outperforms SIC decoding in terms of lower bit error rate at low SNR conditions, while the difference between the two algorithms is not significant at high SNR conditions due to the recursive nature of the forward algorithm.
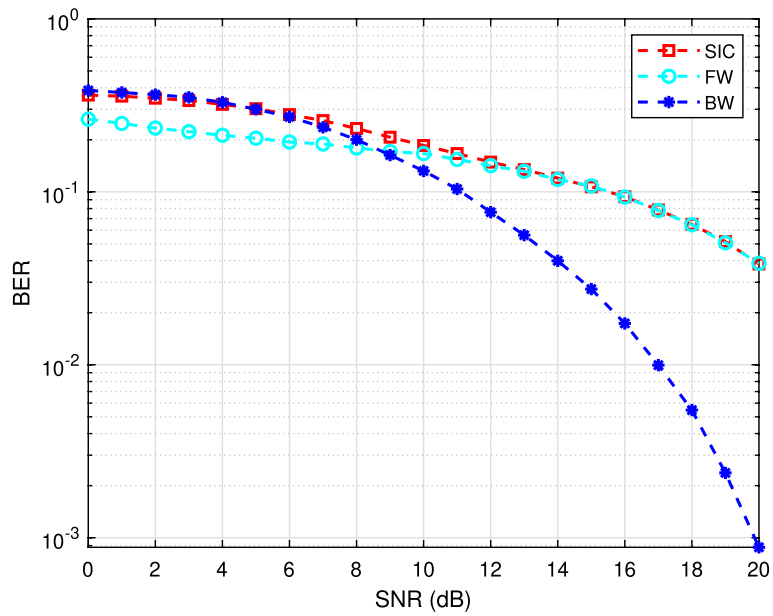
**Fig. 3** Bit error rate of backward and forward algorithm

As shown in 4, FBW was compared with digital video broadcasting (DVB) signals cancellation in [33], FBW partial upgrade compared to DVB signals cancellation. Finally, it is worth mentioning that the backward–forward algorithm first performs backward decoding followed by forward decoding using the obtained label information.
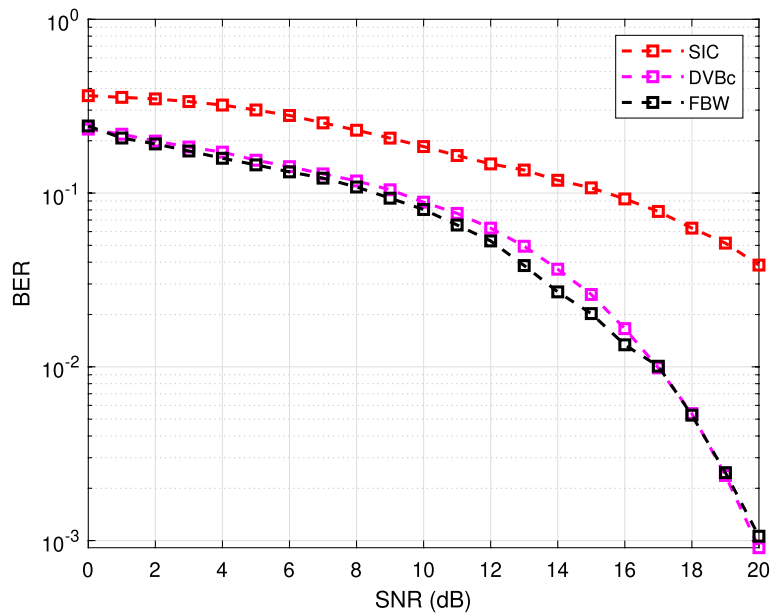


**Fig. 4** Bit error rate of FBW algorithm and DVBc

## 5 Conclusion

This paper has proposed a intelligent backward and forward algorithm for ambient backscatter communication under UAV conditions. The algorithm leverages the retrospective iterative characteristics of the signal and effectively reduces the error bit rate. The separated forced link interference signal can be utilized for energy extraction, achieving the integration of passive communication, interference elimination, and environmental energy harvesting. The results presented in this paper provide valuable insights and methods for the design and optimization of AUAV systems, with significant practical applications in improving system performance.

**Availability of data and materials**
The data that support the findings of this study are available on request from the corresponding author upon reasonable request.

## Declarations

**Ethics approval and consent to participate**
Not applicable.

**Consent for publication**
Not applicable.

**Competing interests**
The authors declare that they have no competing interests.

## References

1. X. Liu, B. Lai, B. Lin, V.C.M. Leung, Joint communication and trajectory optimization for multi-UAV enabled mobile internet of vehicles. IEEE Trans. Intell. Transp. Syst. **23**(9), 15354–15366 (2022)
2. X. Liu, Y. Yu, B. Peng, X.B. Zhai, Q. Zhu, V.C.M. Leung, RIS-UAV enabled worst-case downlink secrecy rate maximization for mobile vehicles. IEEE Trans. Veh. Technol. **72**(5), 6129–6114 (2022)
3. M. Rodríguez, D.P. Tobón, D. Múnera, Anomaly classification in industrial internet of things: a review. Intell. Syst. Appl. **18**(10), 200232 (2023)
4. M.A. Jamshed, K. Ali, Q.H. Abbasi, M.A. Imran, M. Ur-Rehman, Challenges, applications, and future of wireless sensors in internet of things: a review. IEEE Sens. J. **22**(6), 5482–5494 (2022)
5. X. Zhan, H. Guanjie, M. Jia, L. Dong, Potential transmission choice for internet of things (IoT): wireless and batteryless communications and open problems. China Commun. **18**(2), 241–249 (2021)
6. C. Yao, Y. Liu, X. Wei, G. Wang, F. Gao, Backscatter technologies and the future of internet of things: challenges and opportunities. Intell. Converg. Netw. **1**(2), 170–180 (2020)
7. M. Piñuela, P.D. Mitcheson, S. Lucyszyn, Ambient RF energy harvesting in urban and semi-urban environments. IEEE Trans. Microw. Theory Tech. **61**(7), 2715–2726 (2013)
8. X. Zhou, R. Zhang, C.K. Ho, Wireless information and power transfer in multiuser OFDM systems. IEEE Trans. Wireless Commun. **13**(4), 2282–2294 (2014)
9. X. Liu, Z. Liu, B. Lai, B. Peng, T.S. Durrani, Fair energy-efficient resource optimization for multi-UAV enabled internet of things. IEEE Trans. Veh. Technol. **72**(3), 3962–3972 (2022)
10. L. Dai, B. Wang, Z. Ding, Z. Wang, S. Chen, L. Hanzo, A survey of non-orthogonal multiple access for 5G. IEEE Commun. Surve. Tutor. **20**(3), 2294–2323 (2018)
11. Z. Ding, R. Schober, H.V. Poor, Unveiling the importance of SIC in NOMA systems—part 1: state of the art and recent findings. IEEE Commun. Lett. **24**(11), 2373–2377 (2020)

12. C.-B. Le, D.-T. Do, X. Li, Y.-F. Huang, H.-C. Chen, M. Voznak, Enabling NOMA in backscatter reconfigurable intelligent surfaces-aided systems. IEEE Access **9**, 33782–33795 (2021)

13. M. Asif, A. Ihsan, W.U. Khan, A. Ranjha, S. Zhang, S.X. Wu, Energy-efficient backscatter-assisted coded cooperative NOMA for b5G wireless communications. IEEE Trans. Green Commun. Netw. **7**(1), 70–83 (2022)

14. J. Zuo, Y. Liu, L. Yang, L. Song, Y.-C. Liang, Reconfigurable intelligent surface enhanced NOMA assisted backscatter communication system. IEEE Trans. Veh. Technol. **70**(7), 7261–7266 (2021)

15. J. Guo, X. Zhou, S. Durrani, H. Yanikomeroglu, Design of non-orthogonal multiple access enhanced backscatter communication. IEEE Trans. Wirel. Commun. **17**(10), 6837–6852 (2018)

16. J. Guo, S. Durrani, X. Zhou, Monostatic backscatter system with multi-tag to reader communication. IEEE Trans. Veh. Technol. **68**(10), 10320–10324 (2019)

17. W. Chen, H. Ding, S. Wang, D.B. da Costa, F. Gong, P.H. Nardelli, Backscatter cooperation in NOMA communications systems. IEEE Trans. Wirel. Commun. **20**(6), 3458–3474 (2021)

18. H. El Hassani, A. Savard, E.V. Belmega, R.C. De Lamare, Energy-efficient cooperative backscattering closed-form solution for NOMA, in *2021 IEEE Global Communications Conference (GLOBECOM)*. (IEEE, 2021), pp. 1–6

19. G. Wang, F. Gao, R. Fan, C. Tellambura, Ambient backscatter communication systems: detection and performance analysis. IEEE Trans. Commun. **64**(11), 4836–4846 (2016)

20. D. Li, Capacity of backscatter communication with frequency shift in Rician fading channels. IEEE Wirel. Commun. Lett. **8**(6), 1639–1643 (2019)

21. Sung Hoon Kim and Dong In Kim, Hybrid backscatter communication for wireless-powered heterogeneous networks. IEEE Trans. Wirel. Commun. **16**(10), 6557–6570 (2017)

22. J. Qian, F. Gao, G. Wang, S. Jin, H. Zhu, Noncoherent detections for ambient backscatter system. IEEE Trans. Wirel. Commun. **16**(3), 1412–1422 (2016)

23. Q. Zhang, H. Guo, Y.-C. Liang, X. Yuan, Constellation learning-based signal detection for ambient backscatter communication systems. IEEE J. Sel. Areas Commun. **37**(2), 452–463 (2018)

24. R. Duan, R. Jäntti, H. Yiğitler, K. Ruttik, On the achievable rate of bistatic modulated rescatter systems. IEEE Trans. Veh. Technol. **66**(10), 9609–9613 (2017)

25. R. Duan, E. Menta, H. Yigitler, R. Jantti, Z. Han, Hybrid beamformer design for high dynamic range ambient backscatter receivers, in *2019 IEEE International Conference on Communications Workshops (ICC Workshops)*. (IEEE, 2019), pp. 1–6

26. G. Yang, Y.C. Liang, Backscatter communications over ambient OFDM signals: transceiver design and performance analysis, in *2016 IEEE Global Communications Conference (GLOBECOM)*. (IEEE, 2016), pp. 1–6

27. G. Yang, Y.-C. Liang, R. Zhang, Y. Pei, Modulation in the air: backscatter communication over ambient OFDM carrier. IEEE Trans. Commun. **66**(3), 1219–1233 (2017)

28. G. Yang, D. Yuan, Y.-C. Liang, R. Zhang, V.C.M. Leung, Optimal resource allocation in full-duplex ambient backscatter communication networks for wireless-powered IoT. IEEE Internet Things J. **6**(2), 2612–2625 (2018)

29. D. Bharadia, K.R. Joshi, M. Kotaru, S. Katti, Backfi: high throughput wifi backscatter. ACM SIGCOMM Comput. Commun. Rev. **45**(4), 283–296 (2015)

30. S. Gong, J. Xu, L. Gao, X. Huang, W. Liu, Passive relaying scheme via backscatter communications in cooperative wireless networks, in *2018 IEEE Wireless Communications and Networking Conference (WCNC)*. (IEEE, 2018), pp. 1–6

31. B. Lyu, Z. Yang, H. Guo, F. Tian, G. Gui, Relay cooperation enhanced backscatter communication for internet-of-things. IEEE Internet Things J. **6**(2), 2860–2871 (2018)

32. B. Lyu, D.T. Hoang, Z. Yang, User cooperation in wireless-powered backscatter communication networks. IEEE Wirel. Commun. Lett. **8**(2), 632–635 (2019)

33. W. Guo, H. Zhao, C. Song, S. Shao, Y. Tang, Direct-link interference cancellation design for backscatter communications over ambient DVB signals. IEEE Trans. Broadcast. **68**(2), 317–330 (2022)

## Publisher's Note